Journal of Power Sources 483 (2021) 229202

Contents lists available at ScienceDirect

Journal of Power Sources

journal homepage: www.elsevier.com/locate/jpowsour

Asymmetric cycling of vanadium redox flow batteries with a poly(arylene piperidinium)-based anion exchange membrane

Amirreza Khataee [a,*], Dong Pan [b], Joel S. Olsson [b], Patric Jannasch [b], Rakel Wreland Lindström [a]

[a] Applied Electrochemistry, Department of Chemical Engineering, KTH Royal Institute of Technology, SE-100 44, Stockholm, Sweden
[b] Department of Chemistry, Lund University, P.O. Box 124, SE-221 00, Lund, Sweden

HIGHLIGHTS

- Poly (terphenyl)-based AEMs carrying piperidinium cations were fabricated.
- The AEMs showed a significantly low vanadium permeability.
- The AEMs exhibited outstanding resistance against oxidation in the VO_2^+ solution.
- No backbone degradation or ionic loss was recorded for AEMs during VRFB cycling.
- Asymmetric cycling of the VRFB exhibited a capacity decay rate of 0.03% cycle^{-1}.

GRAPHICAL ABSTRACT

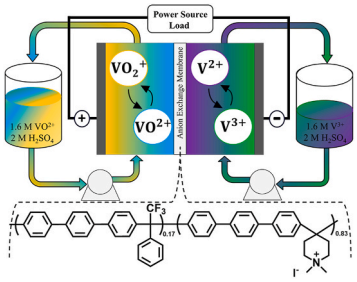

ARTICLE INFO

Keywords:
Vanadium redox flow battery
Anion exchange membrane
Asymmetric cycling
Nafion
Poly (arylene piperidinium)
Piperidinium cations

ABSTRACT

The potential application of a 50 μm thick anion exchange membrane prepared based on poly(terphenyl piperidinium-*co*-trifluoroacetophenone) (PTPT) is investigated for vanadium redox flow batteries (VRFBs). The PTPT exhibits a considerably lower vanadium permeation than Nafion 212. Therefore, the self-discharge duration of the VRFB based on PTPT is much longer than the VRFB based on Nafion 212. Besides, PTPT shows oxidative stability almost as good as Nafion 212 during immersion in an ex-situ immersion test for more than 400 h. Comparing the VRFB performance when symmetric and asymmetric electrolyte volumes are used yields interesting results. The results show that asymmetric cycling is more effective and efficient for the VRFB assembled with PTPT than Nafion 212 as the capacity fade of 0.03% cycle^{-1}, and the highest coulombic efficiency of 98.8% is attained. Furthermore, the color change of the membrane during cycling can be reversed using a straightforward post-treatment method.

1. Introduction

Due to the intermittent nature of renewable energy sources, e.g., solar and wind, and the mismatch between production and consumption, the utilization of these energy sources in the grid depends on the availability of appropriate electrical energy storage technologies. Among various energy storage technologies, electrochemical devices have gained a lot of interest, especially redox flow batteries (RFBs) [1–6]. In general, RFBs offer several significant advantages, including separate scaling of energy and power, long calendar lifetime, stable performance under deep discharge cycling, flexibility in configuration, and low maintenance costs [2,3,6–8]. The all-vanadium redox flow

* Corresponding author.
E-mail address: khat@kth.se (A. Khataee).

https://doi.org/10.1016/j.jpowsour.2020.229202
Received 22 May 2020; Received in revised form 29 October 2020; Accepted 7 November 2020
Available online 17 November 2020
0378-7753/© 2020 The Authors. Published by Elsevier B.V. This is an open access article under the CC BY-NC-ND license (http://creativecommons.org/licenses/by-nc-nd/4.0/).

battery (VRFB) is undoubtedly the most promising and commercially available RFB system [2,3]. Since the same elemental species is used on both sides, not only the cross-contamination of electrolytes is avoided, but also the capacity of the system can be restored by simply remixing the electrolytes [6,9]. Furthermore, compared to traditional lithium-ion batteries, VRFBs are much safer and benefit from the cooling effects of the aqueous electrolytes. Still, VRFBs have a drawback considering the relatively high capital costs (400–800 \$ kWh^{-1}) [10]. Generally, the capital costs of VRFBs are divided into the electrolyte (~40%), stack (~35%), and balance of plant (~25%) [10,11]. The stack part is further sub-divided into three components: membrane, bipolar plates and electrodes [10,12]. Nafion is considered the benchmark cation exchange membrane (CEM) because it shows excellent chemical and mechanical stability owing to its polytetrafluoroethylene (Teflon) backbone and provides high ion conductivity due to the presence of terminal sulfonic acid functional groups. On the other hand, the price of the Nafion membrane is very high [13]. In a VRFB based on Nafion, around 30% of stack costs originate from this component [10]. Another significant issue for the Nafion membrane is the low ion selectivity that imposes severe capacity fade on the VRFB during long-term operation. The latter is due to the large hydrophilic ionic clusters (4–5 nm) of hydrated Nafion, which facilitates the crossover of vanadium ions and water molecules [14]. Some successful attempts have been made to reduce vanadium crossover and enhance the ion selectivity by the composite assembly, layer-by-layer design and nanoparticles impregnation; however, at the cost of reduced ionic conductivity [15].

To achieve superior electrochemical properties, while ensuring that VRFBs are economically competitive with other energy storage technologies in the long-term (to meet the cost target of 150 \$ kWh^{-1}), the development of alternative membranes to Nafion is necessary [16]. Ideally, an ion exchange membrane for a VRFB should be low-cost and chemically robust against oxidation by VO_2^+. Also, it should be efficient in ionic conductivity to maintain high voltage efficiency and ion selectivity to suppress electrolyte imbalance.

Novel non-fluorinated anion exchange membranes (AEMs) have attracted a lot of attention for VRFB and fuel cell applications, and seem to fulfill the requirements mentioned above [13,15,17,18]. Generally, the primary advantage of AEMs over CEMs is the exclusion of vanadium ions from the membrane phase since vanadium ions carrying the same charge as functional groups of AEMs (Donnan exclusion effect). In this way, differential vanadium crossover is reduced, which eventually results in high coulombic efficiency and long self-discharge duration of the VRFB. Also, membrane degradation via chemical oxidation by VO_2^+ is minimized. The two main challenges associated with AEMs are insufficient ionic conductivity (low mobility of anions) and limited chemical stability under harsh conditions. Aliphatic and aromatic backbones carrying various cations, including ammonium, pyridinium and imidazolium, have been studied on non-fluorinated AEMs [15,18,19]. Aliphatic backbones such as polyethylene and even fluorinated ones [e.g., poly(ethylene-*co*-tetrafluoroethylene)] generally have poor chemical stability when in contact with vanadium electrolytes; hence the attention has been turned to aromatic backbones [19,20]. Among the aromatic backbones, polysulfone-based ones undergo degradation in contact with VO_2^+ solution. For example, Yuan et al. reported the performance of a polysulfone-based AEM containing internal cross-linking networks [21]. Despite the cross-linking, the AEM disintegrated after 18 days of immersion in the VO_2^+ solution. The authors attributed the degradation to the interaction between the ether group and lone-pair electrons of the VO_2^+ ion. This is confirmed by the oxidation stability test of poly(phenyl sulfone)-based AEM with pyridinium functional groups in the VO_2^+ solution where the concentration of VO^{2+} during a 450 h oxidation was significantly increased [22].

To address this issue, AEMs based on ether-free poly(phenyl)-based backbones have been reported that show competitive chemical stability and even competitive ionic conductivity compared to Nafion [13,15,18,19]. Recently, Wang et al. investigated the performance of a quaternary ammonium AEM based on poly(terphenyl) in the VRFB [23]. The AEM exhibited low vanadium crossover and 100 stable cycles with high coulombic efficiency (>97%). Also, low area resistance and good oxidation stability in VO_2^+ solution were achieved. Poly(terphenyl) carrying imidazolium cations was also investigated in VRFB and demonstrated excellent oxidation stability for 19 days, a coulombic efficiency of 99.4% and a 3.3 times lower self-discharge rate than Nafion [24]. Furthermore, Zeng et al. reported a pyridinium-functionalized AEM based on a crosslinked network of poly(2,6-dimethyl-1,4-phenylene oxide) [25]. The AEM showed excellent stability during both ex-situ (20 days) and in-situ (537 cycles) tests. Also, due to low vanadium permeability rate, low capacity loss but high coulombic efficiency was achieved.

The unwanted transport of vanadium ions together with water molecules through the membrane has a significant effect on the long-term cycle life of the VRFBs. AEMs suppress the vanadium crossover to a certain extent due to the Donnan exclusion effect. Still, to further minimize the crossover of active species in VRFBs, different concepts have been presented, including asymmetric currents [26], asymmetric volumes [27–29], auto-rebalancing by a hydraulic shunt [30], and using a combination of AEM and CEM [30]. Among the concepts, the use of asymmetric volumes is efficient, uncomplicated, and easy to implement, where depending on the ion exchange membrane type, the capacity fade limiting side has a 10–30% excess volume. Previous studies [27–29] show that VRFBs using electrolytes with asymmetric volumes demonstrate significantly longer cycle life compared to symmetric configuration.

Inspired by the studies mentioned above, the poly(terphenyl) backbone is not readily degraded in contact with vanadium electrolytes and was thus selected in this work. The present study investigates the electrochemical performance of a poly(terphenyl piperidinium-*co*-trifluoroacetophenone) (PTPT) AEM which has previously been studied alkaline membrane fuel cells [31–34]. However, this is the first report on a polyterphenyl-based AEM with piperidinium cations for VRFBs. The membrane was characterized both in-situ and ex-situ and its performance compared with that of Nafion 212. The VRFB measurements were conducted based on the concept of the asymmetric volumes to minimize the capacity fade and improve the performance compared with the symmetric configuration.

2. Experimental

2.1. Materials

Vanadium(V) oxide (V_2O_5, 99.2%) and Vanadium (IV) sulfate oxide hydrate ($VOSO_4$, 99.9%) was obtained from Thermo Fisher Scientific. Vanadium electrolyte containing 1.6 M mixture of $V_2(SO_4)_3$ and $VOSO_4$ in 2 M H_2SO_4 was supplied by GfE company (Gesellschaft für Elektrometallurgie mbH). Magnesium sulfate ($MgSO_4$, ≥99.5%) was purchased from Sigma-Aldrich. Carbon papers (GDL, Sigracet 29 BC) and Nafion 212 membrane were supplied from FuelCellStore. All chemicals for the synthesis of the membrane were purchased from Sigma-Aldrich, VWR, Acros, and TCI and used as received.

2.2. Synthesis of PTPT

The synthesis of PTPT was performed in two steps by a modified previously published procedure [32,33]. First, a precursor polymer was prepared by an acid-catalyzed polyhydroxylalkylation reaction. To a mechanically stirred mixture of *N*-methyl-4-piperidone (mPip, 7.62 mmol), *p*-terphenyl (8.96 mmol) and 2,2,2-trifluoroacetophenone (TFAp, 1.34 mmol) in dichloromethane (DCM, 7.5 mL) at 0 °C, 1,1,1-trifluoroacetic (TFA, 7.84 mmol) and trifluoromethanesulfonic acid (TFSA, 7.5 mL, 84.95 mmol) were added dropwise. After 24 h at 0 °C, the reaction was stopped by precipitation in aq. ethanol. The polymer was washed several times in water and 0.5 M K_2CO_3 at 50 °C and obtained in

quantitative yield after drying. Analysis by ^{1}H NMR spectroscopy showed that the mole fraction of mPip units in the precursor polymer was 0.83. The non-protonated precursor polymer was readily soluble in chloroform, and the protonated form was soluble in dimethyl sulfoxide (DMSO) and *N*-methyl-2-pyrrolidone (NMP). Thermal analysis revealed a glass transition temperature (T_g) and thermal decomposition temperature ($T_{d,95}$) at 357 and 418 °C, respectively.

In the second step, PTPT was prepared by quaternization of the piperidine groups. To a mixture of the precursor polymer (6.21 mmol) in DMSO, K_2CO_3 (2.75 mmol) and iodomethane (16.06 mmol) were added. The reaction solution was stirred in the dark overnight before precipitation in isopropanol. The resulting yellowish polymer powder was then filtered and washed with diethyl ether several times and dried under vacuum at room temperature. PTPT was soluble in DMSO and NMP, but not in chloroform. The thermal stability of PTPT showed $T_{d,95} = 225$ °C. No glass transition was observed below $T_{d,95}$.

2.3. Membrane preparation

AEMs were prepared by solvent casting from 5 wt% polymer in DMSO solutions. The polymer solutions were filtered through a Teflon syringe filter (Millex LS, 5 μm) onto Petri dishes (Ø = 5 cm) before casting at 85 °C for 48 h. To peel off the obtained AEMs from the Petri dish, they were immersed in water. The PTPT AEMs in the chloride form were prepared through ion exchange at 50 °C in 1 M aq. NaCl for 3–5 days. The solution was replaced at least two times during the ion exchange procedure, and the membranes were stored in deionized water between the subsequent measurements.

2.4. Ex-situ characterizations

2.4.1. Water uptake (WU%)

The water uptake of PTPT and Nafion 212 was measured in 2 M H_2SO_4. The ion exchange process was undertaken for 5 days at 40 °C by refreshing the solution three times. The membranes were weighed quickly after wiping off excess liquids on their surface (m_{wet}) and were kept at room temperature for at least 4 h. After subsequent drying at 110 °C for 2 h, the membranes were weighed in a closed vessel (m_{dry1}). To remove excess ions from the acidic electrolyte, samples were washed with deionized water at 75 °C overnight, followed by drying at 110 °C for 2 h and weighing (m_{dry2}). The water uptake was then calculated using the following equation:

$$Water\ uptake\ (WU\%) = \frac{m_{\mathrm{wet}} - m_{\mathrm{dry1}}}{m_{\mathrm{dry2}}} \times 100\% \quad (1)$$

2.4.2. Area specific resistance (ASR) and ionic conductivity

Both Nafion 212 and PTPT were soaked in 2 M H_2SO_4 for one day prior to the ASR measurement. The high-frequency resistance of the RFB system with (R_w) and without (R_{wo}) membrane while 2 M H_2SO_4 circulated was measured by electrochemical impedance spectroscopy (EIS) using a four-probe VersaSTAT 4 workstation at a frequency range of 1 MHz–10 Hz with an amplitude of 5 mV. The measurements were conducted at room temperature. The high-frequency resistance of the membranes was obtained from the difference of R_w and R_{wo}. The ionic conductivity (σ, mS cm^{-1}) was calculated by using the ASR values (Equation (2)):

$$\sigma = \frac{l}{ASR_{hf}} \quad where\ ASR_{hf} = (R_w - R_{wo})\mathrm{A} \quad (2)$$

Here, l and A denote the thickness and the active area of the membrane, respectively.

2.4.3. Ion exchange capacity (IEC)

The IEC (mmol g^{-1}) of PTPT was determined by Mohr titration. PTPT membrane in the bromide form (0.03 g) was first dried under vacuum at 50 °C for 48 h and quickly weighed to obtain the dry weight. Then the membrane was immersed in aq. $NaNO_3$ (0.2 M, 25 mL) and kept in a sealed container at 60 °C for two days. The resulting solution was titrated (5 mL x 4 times) with fresh aq. $AgNO_3$ (0.01 M) using K_2CrO_4 as the colorimetric indicator. The titration endpoint was indicated by the formation of a red precipitate of Ag_2CrO_4.

2.4.4. Permeability of VO^{2+}

Among oxidation states of vanadium, the permeability of VO^{2+} is usually measured because VO^{2+} is a more robust species towards oxidation in air. VO^{2+} permeability through PTPT and Nafion 212 was studied using the permeation cell shown in Fig. S1. Membrane samples with an active area of 8.3 cm^2 were sandwiched between two electrolyte chambers with a volume of 250 mL. The left chamber was filled with 1 M $VOSO_4$ in 2 M H_2SO_4 while the left chamber with 1 M $MgSO_4$ in 2 M H_2SO_4. $MgSO_4$ was used to balance the ion strength and reduce the water transfer due to the osmotic effect. Magnetic stirrers were used in both chambers to avoid concentration polarization. The concentration of VO^{2+} in the right chamber was measured using VersaWave UV–vis spectrometer. The samples (50 μL) were taken at certain time intervals from the right chamber and transferred to 950 μL MilliQ water to reach 20 times dilution. Afterward, each sample's absorbance was measured at 765 nm through a 10 mm light path quartz cuvette. Equation (3) was used to calculate the permeability (P, cm^2 min^{-1}) of VO^{2+}:

$$\boldsymbol{P} = \frac{\mathbf{L}\boldsymbol{V}_{\mathbf{R}}}{\boldsymbol{A}(\boldsymbol{C}_{\mathbf{L}} - \boldsymbol{C}_{\mathbf{R}}(\mathbf{t}))} \frac{\boldsymbol{dC}_{\mathbf{R(t)}}}{\boldsymbol{dt}} \quad (3)$$

where L is the thickness of the membrane, V_R is the volume of the right chamber, A is the active area of the membrane, C_L is the concentration of VO^{2+} in the left chamber, C_R(t) is the concentration of vanadium in the right chamber at the time of t, and t itself is the measurement time.

2.4.5. Oxidation stability

Small pieces of pristine Nafion 212 and PTPT with the same size were immersed in 25 mL of 1.6 M VO_2^+ and 2 M H_2SO_4 solution at room temperature (24 °C) and 30 °C for more than 400 h. The concentration of VO^{2+} in the solution was measured using a UV–vis spectrometer. The samples (50 μL) were taken at certain time intervals from the solution and transferred to 950 μL MilliQ water to reach 20 times dilution. Afterward, the absorbance of each sample was measured at 765 nm through a 10 mm light path quartz cuvette. Moreover, to investigate the structural changes, ^{1}H NMR spectra of immersed PTPT and pristine samples were compared.

2.4.6. Spectroscopy analysis

The Raman spectroscopy was carried out with an HR800 UV Jobin Yvon Raman (Horiba, Kyoto, Japan) instrument in combination with a solid-state laser with a wavelength of 514 nm used with a 100 × objective and a 600-groove mm^{-1} density grating. The spectra were acquired in the range of 400–1800 cm^{-1} with a resolution of 2 cm^{-1}. Up to 10 spectra were accumulated to obtain high signal/noise ratios with a total acquisition time of <1 min ^{1}H NMR spectra of the polymers were recorded on a Bruker DR X400 spectrometer at 400.13 MHz using DMSO-d_6 (δ = 2.50 ppm). TFA was added (5–10 vol%) to move the water peak to above 10 ppm and reveal otherwise hidden proton shifts.

2.5. In-situ characterizations

2.5.1. Flow battery measurements

Charge-discharge cycles of the VRFB were conducted using an electrochemical cell provided by Fuel Cell Technologies (FCT). The cell consists of two Poco graphite plates with a serpentine flow field. Two Viton gaskets with a thickness of 1 mm were used for sealing. Six carbon papers, each with a thickness of 0.22 mm and an area of 5 cm^2, were used as electrodes on both sides of the cell. The electrodes were

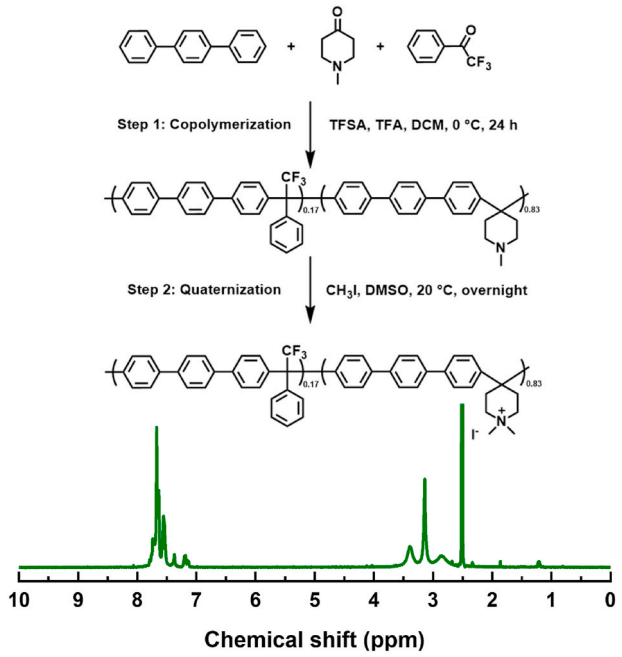

Fig. 1. Synthesis procedure and ^{1}H NMR spectrum of poly (terphenyl piperidinium-*co*-trifluoroacetophenone) (PTPT).

pretreated at 500 °C for 3 h under the air atmosphere. Nafion 212 as cation exchange and PTPT as anion exchange membrane (AEM) were used as the separator. For symmetric tests, 20 mL vanadium electrolytes were used on both negative and positive sides, while in the case of asymmetric tests, the volume of either the positive or negative side was reduced by 25%. The electrolytes were purged with nitrogen for at least 10 min and sealed well to minimize the oxidation of vanadium species prior to each measurement. The electrolytes were circulated at 40 mL min^{-1} using a dual-channel peristaltic pump (BT600L, Zhengzhou Mingyi Instrument Equipment Co., Ltd). All flow battery measurements were carried out at 24 °C. The charge/discharge data were collected using an 8-channel battery test system CT2001A (Landt Instruments) in the four-wire configuration and cut off voltages of 1.7 V and 0.8 V.

Three types of efficiencies called coulombic, voltage, and energy were used to evaluate the VRFB performance. Coulombic efficiency (CE) is the ratio of discharge capacity to charge capacity. Voltage efficiency (VE) is defined as the ratio of average discharge voltage to average charge voltage, and the multiplication of CE by VE calculates the energy efficiency (EE). Also, the rate performance of VRFB was investigated by cycling galvanostatically at current densities from 70 to 200 mA cm^{-2} and returning to 70 mA cm^{-2}. At each current density, 5 charge-discharge cycles were recorded.

Furthermore, polarization curves were measured to calculate the total resistance of the VRFB by the cycling galvanostatically at different current densities (2–400 mA cm^{-2}) and recording the average cell voltage for 1 min. All polarization curve data were recorded at 50% state of charge.

2.5.2. Self-discharge of the VRFB

The self-discharge duration of the VRFB with Nafion 212 or PTPT was investigated by fully charging the system at a relatively low current density of 20 mA cm^{-2} and afterward, leaving the system on open-circuit condition. The open-circuit voltage (OCV) was recorded until reaching a value close to 0 V.

Table 1
Properties of Nafion 212 and PTPT. Water uptake, conductivity, and ASR measured using 2 M H_2SO_4. ASR and conductivity from EIS in RFB setup. Permeability measured in 1 M $VOSO_4$ in 2 M H_2SO_4 | 1 M $MgSO_4$ in 2 M H_2SO_4.

Membrane	Thickness (μm)	Conductivity (mS cm^{-1})	Water uptake (%)	Permeability ($\times 10^{-9}$ cm^2 min^{-1})	ASR (Ω cm^2)
Nafion 212	51	63.7	17	11.200	0.08
PTPT	50	9.4	35	0.428	0.53

3. Results and discussion

3.1. Synthesis and characterization of PTPT

PTPT was synthesized in a superacid-catalyzed polymerization, followed by quaternization with iodomethane, as shown in Fig. 1. The chemical structure of the polymer was confirmed by ^{1}H NMR analysis. All signals from protons located in the aromatic backbone were found between 7 and 8 ppm, while signals from methyl and methylene protons in the piperidinium ring were observed at 3.1 ppm and 2.8 and 3.4 ppm, respectively. The quaternized polymer in the iodide form was cast from DMSO solutions (5 wt%) in Petri dishes at 85 °C during 48 h to form transparent and flexible AEMs. Hence, in the sections below PTPT is in the iodide form, unless otherwise stated. Table 1 presents the key properties of Nafion 212 and PTPT. A high ratio of piperidone to TFAp was selected in the polymerization step of PTPT to achieve sufficient water uptake and conductivity of the AEMs. Accordingly, an IEC value of approximately 2 mmol g^{-1} in the bromide form was obtained, as confirmed by Mohr titration (2.13 mmol g^{-1}). Previous measurements by small-angle X-ray spectroscopy (SAXS) have shown that poly(arylene piperidinium) AEMs do not display any ionomer peaks, unless tethered with long alkyl chains [31,33]. Hence, the ions in these membranes cluster poorly, most likely because of the high stiffness of the aromatic backbone. Although Nafion 212 and PTPT have almost the same thickness and PTPT has a higher ion exchange capacity, the ionic conductivity of Nafion 212 is seven times higher. Generally, both protons and sulfate ions contribute to ionic conductivity. In Nafion 212, predominant charge carriers are protons, while both protons and sulfate ions contribute to the total conductivity in PTPT due to the uptaken acidic electrolyte [25,35]. The mobility of protons is four times higher than sulfate ions [36]. For the same reason and as can be seen in Fig. S2, the ASR of PTPT is higher than Nafion 212.

As electrolyte imbalance is one of the main factors accountable for performance loss in VRFBs, it is of paramount importance to measure the permeation rate of vanadium through the membrane. The permeation rate is a useful index to evaluate the extent of Donnan exclusion. The strong Donnan exclusion effect will enhance the CE and prolong the self-discharge of the VRFB. Fig. 2a and Table 1 show that the VO^{2+} permeation rate through PTPT during 140 h was significantly lower than that of not only Nafion 212 but also the previously reported values for hydrocarbon-based AEMs [19]. Another major factor causing performance loss in VRFBs is membrane degradation via oxidation by VO_2^+. The oxidation stability of PTPT and Nafion 212 was investigated in the VO_2^+ electrolyte, and the results are shown in Fig. 2b. As expected, Nafion 212 with its Teflon backbone showed excellent oxidation resistance. PTPT at room temperature also exhibits outstanding resistance against oxidation for more than 400 h, with less than 1% reduction of VO_2^+ to VO^{2+}. This observation might be explained by a combination of the Donnan exclusion effect and the relatively compact structure of the PTPT backbone. A different trend was observed at 30 °C. The oxidation reaction rate increased, and three times more VO^{2+} was generated for the same duration. Nevertheless, the NMR analysis showed no change in the membrane's chemical structure either at room or elevated temperature (Fig. S3), which confirms the excellent oxidation stability of PTPT.

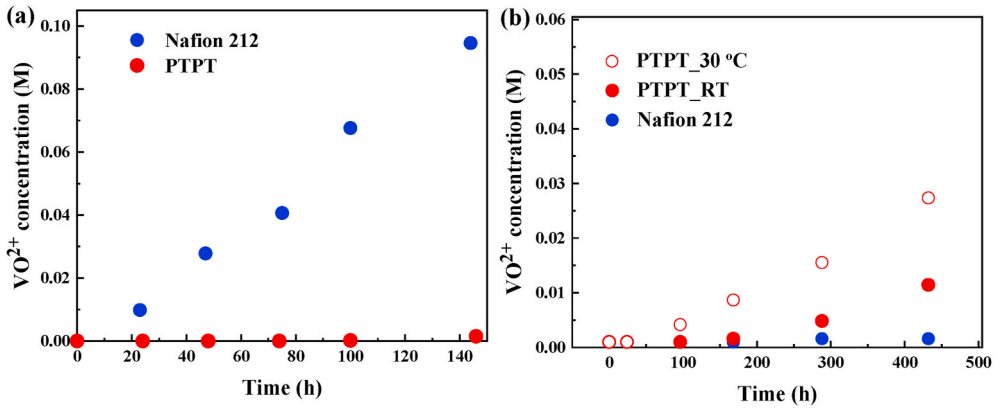

Fig. 2. (a) Permeability measurement of VO^{2+} ion with diffusion cell using ~50 μm Nafion 212 and PTPT ion exchange membranes at room temperature; (b) Measurement of VO^{2+} concentration during immersion of Nafion 212 and PTPT in the high oxidizing electrolyte: 1.6 M VO_2^+ in 2 M H_2SO_4.

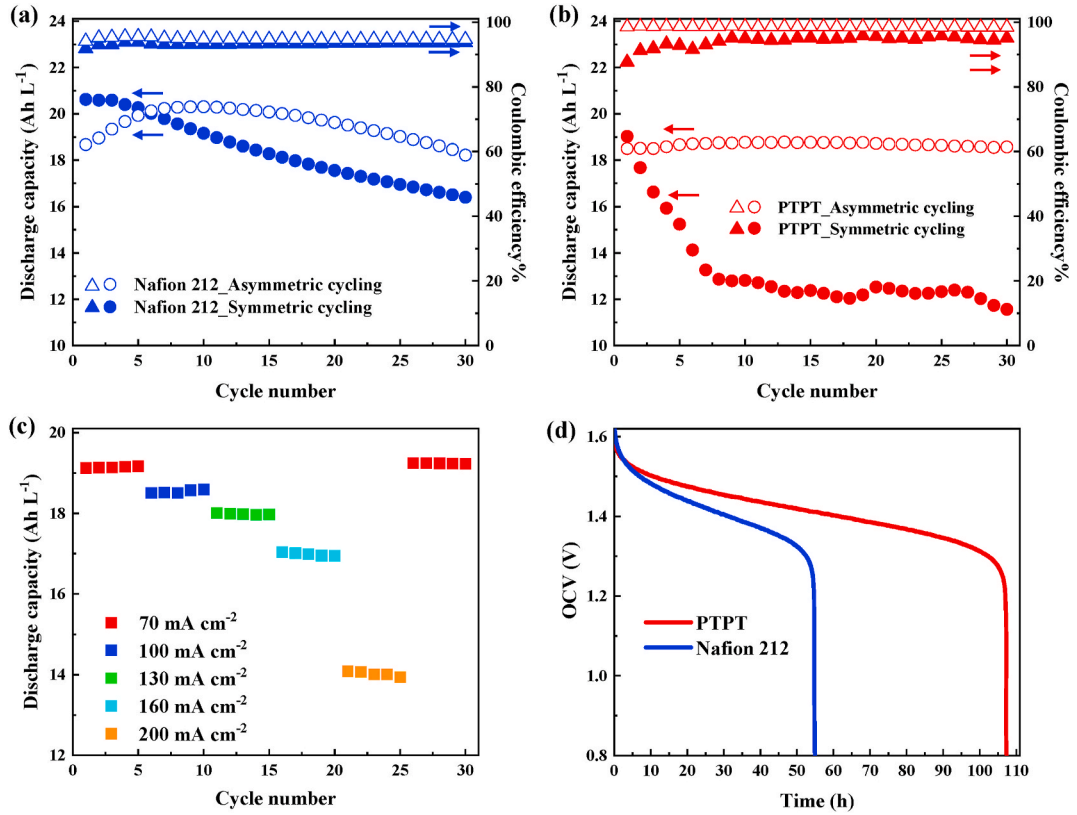

Fig. 3. (a) Symmetric and asymmetric cycling of VRFB using Nafion 212 as ion exchange membrane; (b) Symmetric and asymmetric cycling of VRFB using untreated PTPT as ion exchange membrane; (c) Rate performance of VRFB based on PTPT; (d) Self-discharge duration of Nafion 212 and PTPT in open circuit condition; Experimental conditions: 1.6 M V^{3+} as negative electrolyte and 1.6 M VO^{2+} as positive electrolyte both in 2 M H_2SO_4 as supporting electrolyte. Constant current density of 100 mA cm^{-2}, 40 mL min^{-1} as flow rate and temperature of 24 °C.

Although NMR spectroscopy showed no signs of membrane degradation, the partial oxidation of PTPT cannot be ruled out. The oxidation could be attributed to the reaction of iodide ions within the membrane by VO_2^+ which affects the conductivity of membrane and will be discussed in the following sections.

3.2. Flow battery performance

The in-situ characterization of Nafion 212 and PTPT was investigated by running the cyclic charge-discharge measurements on the VRFB. Fig. 3a shows the cycling results using Nafion 212. The VRFB based on the symmetric volume of electrolytes, provided a CE of 93.3% and discharge capacity fade of 20% (drop from 20.6 Ah L^{-1} to 16.4 Ah L^{-1}). More precisely, the discharge capacity remained constant in the beginning and decreased sharply in the subsequent cycles. The relatively large capacity fade was mainly attributed to the differential crossover of active species. As V^{2+} and V^{3+} have more significant permeability than VO^{2+} and VO_2^+ through the Nafion membrane, the net vanadium diffusion is from the negative to the positive side [37].

On the other hand, considering the ionic current direction, the net vanadium and water transfer under migration and electroosmotic convection is from the positive to the negative side during charging, while in the opposite direction during discharging [38]. It should be noted that water molecules are also transferred together with vanadium cations as

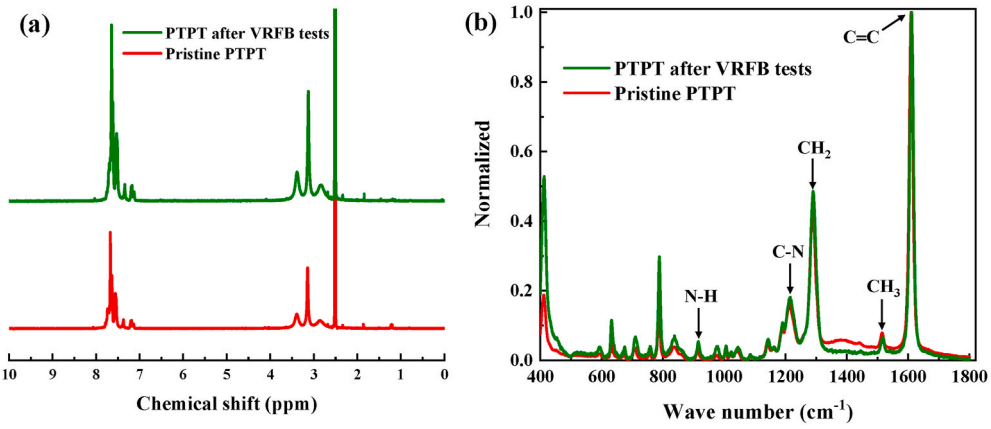

Fig. 4. (a) ^{1}H NMR of PTPT in DMSO-d_6 with TFA added; (b) Raman spectra of PTPT (The spectral data were normalized by the intensity maximum of each spectrum).

each hydrated vanadium cation, depending on the oxidation states, carries 5–6 water molecules [9]. Since all the transfer mechanisms are along the same direction during discharging, the net crossover is said to be from negative to the positive side [38,39]. This was confirmed by the volume increase of 7.5% on the positive side after 30 cycles. The vanadium crossover causes self-discharge of charged vanadium species, which intensifies the capacity fade. For instance, VO^{2+} and VO_2^+ travel through the membrane and react with V^{2+} and V^{3+} according to the reactions below [9,40]:

$$VO^{2+} + 2V^{2+} + 4H^{+} \rightarrow 3V^{3+} + 2H_2O \quad (4)$$

$$VO_2^{+} + 2V^{2+} + 4H^{+} \rightarrow 3V^{3+} + 2H_2O \quad (5)$$

$$VO_2^{+} + V^{3+} \rightarrow 2VO^{2+} \quad (6)$$

Similar reactions occur if the V^{2+} and V^{3+} crossover to the positive side [9,40]:

$$V^{2+} + 2VO_2^{+} + 2H^{+} \rightarrow 3VO^{2+} + H_2O \quad (7)$$

$$V^{3+} + VO_2^{+} \rightarrow 2VO^{2+} \quad (8)$$

$$V^{2+} + VO^{2+} + 2H^{+} \rightarrow 2V^{3+} + H_2O \quad (9)$$

From the above explanation, it is obvious that the negative electrolyte limits the capacity of VRFB using Nafion 212. According to the asymmetric volume concept, 25% excess volume was used on the negative side to hinder the capacity fade. Referring again to Fig. 3a, the CE achieved for asymmetric cycling was as high as symmetric. However, the discharge capacity was differently altered. There are two steps in the discharge capacity curve: a gradual increase in the beginning, then a slow decrease. During the first step, the capacity was limited by the positive electrolyte, and considering the net crossover direction in Nafion 212, active species accumulated in the positive side and decreased in the negative side. When the capacity reached the summit, the negative electrolyte became the limiting factor. In the second step, the equilibrium state was established, which slows down the capacity fade compared to the symmetric cycling.

Following these results, a VRFB using PTPT was also operated in both symmetric and asymmetric configurations, as shown in Fig. 3b. The symmetric measurements showed an average CE of 94.17%, which is slightly higher than the results with Nafion 212, although PTPT showed a strong Donan exclusion effect (Fig. 2a). This is because electrolyte imbalance still occurred due to severe non-equilibrium water transport as a result of high water uptake. This effect is visible in the first a few cycles of the discharge capacity curve. Before discussing the results of the asymmetric measurements, it is important to review the net crossover direction in AEMs. The permeability of VO^{2+} and VO_2^+ across AEMs are usually larger than those of V^{2+} and V^{3+}, meaning that the net vanadium diffusion direction is from positive to the negative side [37,38].

On the other hand, net migration and electroosmotic convection of vanadium ions and water are along the same direction as the ionic current from positive to negative side during charging [38]. As all transfer mechanisms have the same direction during charging, the net crossover is, therefore, being considered towards the negative side. The 7% volume increase of the negative electrolyte after 30 cycles confirms the latter claim. Accordingly, asymmetric cycling measurements were configured by using 25% excess volume on the positive side. Unlike Nafion 212, the asymmetric cycling using PTPT showed higher CE (98.5%) than symmetric and the highest CE of 98.8% was achieved at the current density of 160 mA cm^{-2}. Consequently, the energy efficiency of asymmetric cycling, as shown in Fig. S4, is higher than symmetric tests.

It should be noted that the lower discharge capacity compared to Nafion 212 is due to the lower conductivity of PTPT, which increases the polarization effect and eventually shortens the charge-discharge cycles (Fig. S5). Impressive results were observed by measuring the discharge capacity. Surprisingly, the capacity fade for asymmetric tests decreased significantly compared to symmetric, i.e., 1% for 30 cycles. Obviously, using asymmetric volumes suppressed the water crossover, and the equilibrium state of electrochemical reactions was established from the initial cycles. These results strongly suggest that, in similar experimental conditions, using the asymmetric volume concept on VRFB using PTPT with high water uptake value was more beneficial than Nafion 212 in boosting the CE and reducing the capacity fade. Due to the very low crossover rate using asymmetric volumes, excellent rate performance was observed for the VRFB based on PTPT (Fig. 3c). As can be seen, the VRFB exhibits an outstanding capacity retention capability by increasing current density from 70 to 200 mA cm^{-2} and decreasing once again to 70 mA cm^{-2}. In fact, the capacity does not drop a lot by a sudden variation of the current density. It is good to mention that capacity reduction by increasing current density is because the polarization becomes more pronounced at high current densities. The self-discharge of VRFB or consumption of V^{2+} and VO_2^+ in the negative and positive electrolyte, respectively, took 55 h for Nafion 212 and 107 h for PTPT (Fig. 3d). These results are in excellent agreement with the results of the permeability measurement shown in Fig. 2a and asymmetric cycling tests in Fig. 3b. The chemical stability of PTPT was investigated by NMR and RAMAN spectroscopy (Fig. 4a and b, respectively). The RAMAN intensity peaks corresponding to the C-C and C=C vibrations of phenyl rings are observed in 1591-1068 cm^{-1} and 1610 cm^{-1}, respectively, and remained unchanged after VRFB cycling [41]. Also, the intensity of vibration of N-H, C-N and CH_3 correspond to the

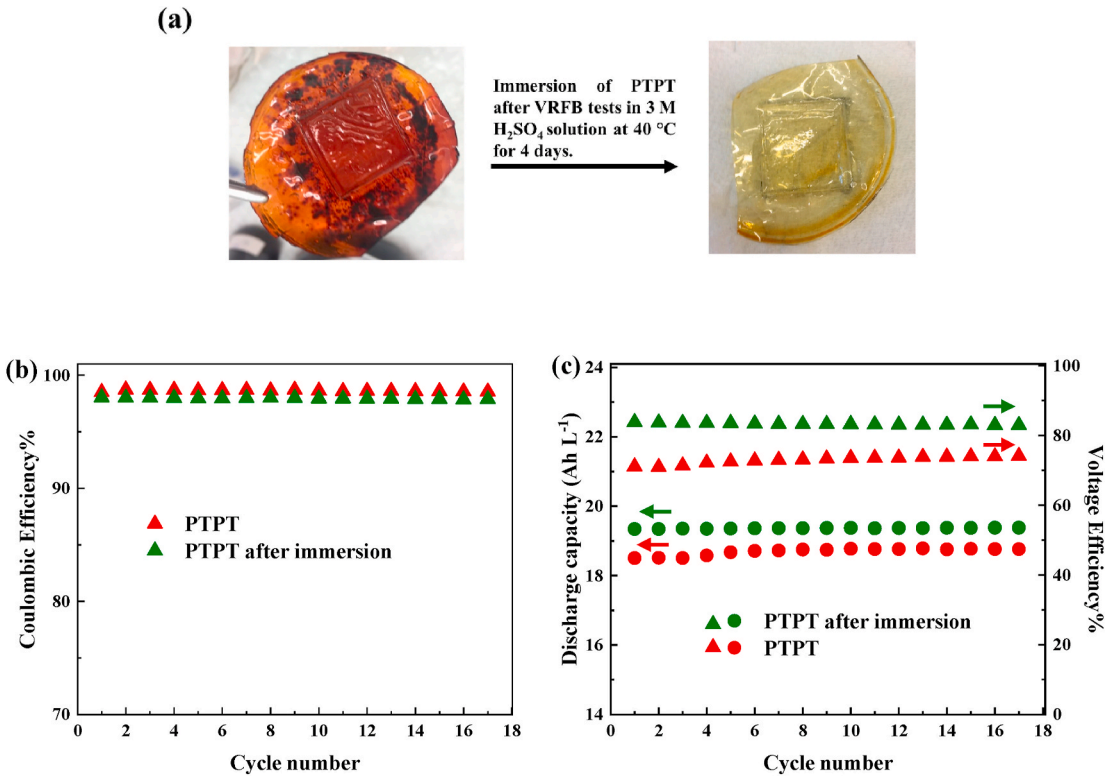

Fig. 5. Performance improvement of VRFB after immersion of PTPT in an acidic solution: (a) Color change after immersion; (b) Discharge capacity and voltage efficiency comparison and (c) Coulombic efficiency comparison. (For interpretation of the references to color in this figure legend, the reader is referred to the Web version of this article.)

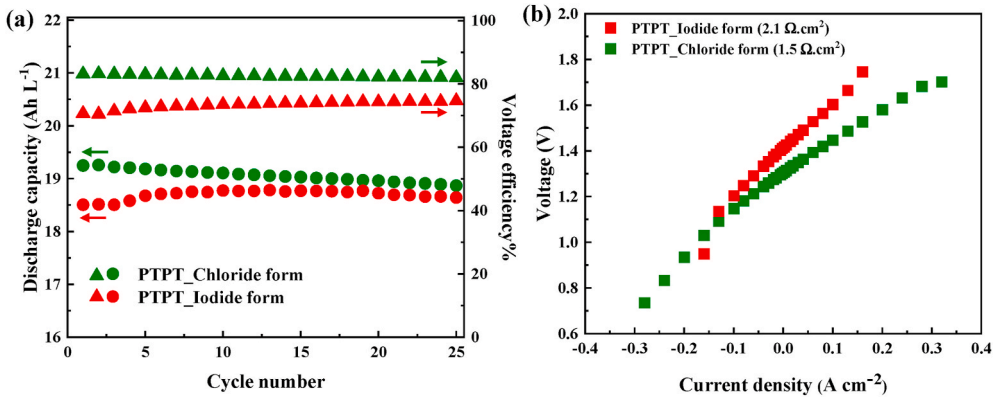

Fig. 6. VRFB asymmetric cycling by using PTPT in chloride and iodide form; (a) Discharge capacity and voltage efficiency versus cycle number and (b) Polarization curves of VRFB based on PTPT in chloride and iodide forms at 50% SOC.

piperidinium group is the same for the pristine and used membrane [41]. Overall, the results showed that the integrity of the polymer backbone and piperidinium functional groups remained unchanged after VRFB cycling, which is in accordance with oxidation stability results demonstrated in Fig. 2b. The long-term reproducibility of asymmetric cycling using PTPT is demonstrated in Fig. S6. The small capacity fade of ~4% denotes that the membrane remains stable in long-term tests as well. It should also be pointed out that the membrane color changed from yellowish in the beginning to reddish after VRFB cycling, most likely due to the iodide oxidation and complex formation within the membrane. However, the color returned to the initial yellowish by immersing used PTPT in 3 M sulfuric acid at 40 °C for 4 days (Fig. 5a). As can be seen in Fig. 5b and c, the VRFB using the immersed membrane showed the same CE, but superior VE and discharge capacity. This is indeed an exciting result, which suggests that the absence of iodide contamination could increase the conductivity of the PTPT. To confirm this claim, a PTPT was prepared in the chloride form and the performance investigated in a VRFB under the same experimental conditions. The asymmetric cycling tests demonstrated higher voltage efficiency and higher discharge capacity over PTPT (Fig. 6a). The polarization curves comparison in Fig. 6b demonstrates lower resistance for PTPT in chloride form. Lastly, almost the same CE was achieved for both membranes (Fig. S7). More importantly, the color of PTPT in chloride form did not change after VRFB cycling tests.

4. Conclusions

A novel anion exchange membrane with a poly(terphenyl) backbone

and piperidinium functional groups (PTPT) was synthesized and evaluated in the VRFB. The PTPT membrane demonstrated significantly lower vanadium permeability than Nafion 212. Besides, the oxidation stability of PTPT was as good as Nafion 212 in the VO_2^+ solution. The high water uptake of the PTPT membrane led to severe non-equilibrium water crossover and electrolyte imbalance during VRFB cycling; however, cycling based on asymmetric electrolyte volumes significantly reduced the capacity loss. Accordingly, a high coulombic efficiency of 98.8% and excellent rate performance were achieved. It was supported by NMR and Raman spectroscopy that no backbone degradation or ionic loss was detected for PTPT during VRFB cycling. Finally, any presence of iodide within the membrane contributed to a reduced ionic conductivity and voltage efficiency.

CRediT authorship contribution statement

Amirreza Khataee: Conceptualization, Methodology, Validation, Investigation, Writing - original draft, Writing - review & editing. **Dong Pan:** Validation, Writing - review & editing, Investigation. **Joel S. Olsson:** Validation, Writing - review & editing, Investigation. **Patric Jannasch:** Writing - review & editing, Supervision, Funding acquisition. **Rakel Wreland Lindström:** Writing - review & editing, Supervision, Funding acquisition.

Declaration of competing interest

The authors declare that they have no known competing financial interests or personal relationships that could have appeared to influence the work reported in this paper.

Acknowledgments

This work was supported by Batterifonden via Swedish Energy Agency and StandUp for Energy (Grant agreement no. 45515-1). The authors also would like to thank Jonas Garemark for the experimental support during the Raman spectroscopy time.

Appendix A. Supplementary data

Supplementary data to this article can be found online at https://doi.org/10.1016/j.jpowsour.2020.229202.

References

[1] R.H. Byrne, T.A. Nguyen, D.A. Copp, B.R. Chalamala, I. Gyuk, IEEE Access 6 (2018) 13231–13260, https://doi.org/10.1109/ACCESS.2017.2741578.
[2] B. Dunn, H. Kamath, J.-M. Tarascon, Science 334 (2011) 928, https://doi.org/10.1126/science.1212741.
[3] J. Cho, S. Jeong, Y. Kim, Prog. Energy Combust. Sci. 48 (2015) 84–101, https://doi.org/10.1016/j.pecs.2015.01.002.
[4] L.F. Arenas, C. Ponce de León, F.C. Walsh, Curr. Opin. Electrochem. 16 (2019) 117–126, https://doi.org/10.1016/j.coelec.2019.05.007.
[5] H. Zhang, W. Lu, X. Li, Electrochem. Energy Rev. 2 (2019) 492–506, https://doi.org/10.1007/s41918-019-00047-1.
[6] P. Leung, X. Li, C. Ponce de León, L. Berlouis, C.T.J. Low, F.C. Walsh, RSC Adv. 2 (2012) 10125–10156, https://doi.org/10.1039/C2RA21342G.
[7] A. Poullikkas, Renew. Sustain. Energy Rev. 27 (2013) 778–788, https://doi.org/10.1016/j.rser.2013.07.017.
[8] A.Z. Weber, M.M. Mench, J.P. Meyers, P.N. Ross, J.T. Gostick, Q. Liu, J. Appl. Electrochem. 41 (2011) 1137, https://doi.org/10.1007/s10800-011-0348-2.
[9] C. Choi, S. Kim, R. Kim, Y. Choi, S. Kim, H.-y. Jung, J.H. Yang, H.-T. Kim, Renew. Sustain. Energy Rev. 69 (2017) 263–274, https://doi.org/10.1016/j.rser.2016.11.188.
[10] C. Minke, T. Turek, J. Power Sources 376 (2018) 66–81, https://doi.org/10.1016/j.jpowsour.2017.11.058.
[11] M. Moore, R. Counce, J. Watson, T. Zawodzinski, J. Adv. Chem. Eng. 5 (2015) 1–3, https://doi.org/10.4172/2090-4568.1000140.
[12] J. Xi, B. Jiang, L. Yu, L. Liu, J. Membr. Sci. 522 (2017) 45–55, https://doi.org/10.1016/j.memsci.2016.09.012.
[13] X. Li, H. Zhang, Z. Mai, H. Zhang, I. Vankelecom, Energy Environ. Sci. 4 (2011) 1147–1160, https://doi.org/10.1039/C0EE00770F.
[14] K.A. Mauritz, R.B. Moore, Chem. Rev. 104 (2004) 4535–4586, https://doi.org/10.1021/cr0207123.
[15] T.N.L. Doan, T.K.A. Hoang, P. Chen, RSC Adv. 5 (2015) 72805–72815, https://doi.org/10.1039/C5RA05914C.
[16] U.S. Department of Energy, Grid energy storage report. https://www.energy.gov/oe/downloads/grid-energy-storage-december-2013 accessed accessed December 2013.
[17] Y. Shi, C. Eze, B. Xiong, W. He, H. Zhang, T.M. Lim, A. Ukil, J. Zhao, Appl. Energy 238 (2019) 202–224, https://doi.org/10.1016/j.apenergy.2018.12.087.
[18] S. Maurya, S.-H. Shin, Y. Kim, S.-H. Moon, RSC Adv. 5 (2015) 37206–37230, https://doi.org/10.1039/C5RA04741B.
[19] L. Zeng, T.S. Zhao, L. Wei, H.R. Jiang, M.C. Wu, Appl. Energy 233–234 (2019) 622–643, https://doi.org/10.1016/j.apenergy.2018.10.063.
[20] S.-J. Seo, B.-C. Kim, K.-W. Sung, J. Shim, J.-D. Jeon, K.-H. Shin, S.-H. Shin, S.-H. Yun, J.-Y. Lee, S.-H. Moon, J. Membr. Sci. 428 (2013) 17–23, https://doi.org/10.1016/j.memsci.2012.11.027.
[21] Z. Yuan, X. Li, Y. Zhao, H. Zhang, ACS Appl. Mater. Interfaces 7 (2015) 19446–19454, https://doi.org/10.1021/acsami.5b05840.
[22] B. Zhang, E. Zhang, G. Wang, P. Yu, Q. Zhao, F. Yao, J. Power Sources 282 (2015) 328–334, https://doi.org/10.1016/j.jpowsour.2015.02.070.
[23] T. Wang, J.Y. Jeon, J. Han, J.H. Kim, C. Bae, S. Kim, J. Membr. Sci. (2019), 117665, https://doi.org/10.1016/j.memsci.2019.117665.
[24] B. Shanahan, T. Böhm, B. Britton, S. Holdcroft, R. Zengerle, S. Vierrath, S. Thiele, M. Breitwieser, Electrochem. Commun. 102 (2019) 37–40, https://doi.org/10.1016/j.elecom.2019.03.016.
[25] L. Zeng, T.S. Zhao, L. Wei, Y.K. Zeng, Z.H. Zhang, J. Power Sources 331 (2016) 452–461, https://doi.org/10.1016/j.jpowsour.2016.09.065.
[26] E. Agar, A. Benjamin, C.R. Dennison, D. Chen, M.A. Hickner, E.C. Kumbur, in: 224th ECS Meeting, The Electrochemical Society, 2013, 1662-1662.
[27] W. Lee, M. Jung, D. Serhiichuk, C. Noh, G. Gupta, C. Harms, Y. Kwon, D. Henkensmeier, J. Membr. Sci. 591 (2019), 117333, https://doi.org/10.1016/j.memsci.2019.117333.
[28] D. Mu, Y. Zhao, L. Yu, L. Liu, J. Xi, Phys. Chem. Chem. Phys. 19 (2017) 29195–29203, https://doi.org/10.1039/C7CP06249D.
[29] J.H. Park, J.J. Park, O.O. Park, J.H. Yang, ChemSusChem 9 (2016) 3181–3187, https://doi.org/10.1002/cssc.201601110.
[30] A. Bhattarai, P. Ghimire, A. Whitehead, R. Schweiss, G. Scherer, N. Wai, H. Hng, Batteries 4 (2018) 48, https://doi.org/10.3390/batteries4040048.
[31] J.S. Olsson, T.H. Pham, P. Jannasch, J. Membr. Sci. 578 (2019) 183–195, https://doi.org/10.1016/j.memsci.2019.01.036.
[32] J. Wang, Y. Zhao, B.P. Setzler, S. Rojas-Carbonell, C. Ben Yehuda, A. Amel, M. Page, L. Wang, K. Hu, L. Shi, S. Gottesfeld, B. Xu, Y. Yan, Nat. Energy 4 (2019) 392–398, https://doi.org/10.1038/s41560-019-0372-8.
[33] J.S. Olsson, T.H. Pham, P. Jannasch, Adv. Funct. Mater. 28 (2018), 1702758, https://doi.org/10.1002/adfm.201702758.
[34] H. Peng, Q. Li, M. Hu, L. Xiao, J. Lu, L. Zhuang, J. Power Sources 390 (2018) 165–167, https://doi.org/10.1016/j.jpowsour.2018.04.047.
[35] D. Chen, M.A. Hickner, E. Agar, E.C. Kumbur, Electrochem. Commun. 26 (2013) 37–40, https://doi.org/10.1016/j.elecom.2012.10.007.
[36] A.J. Bard, L.R. Faulkner, J. Leddy, C.G. Zoski, Electrochemical Methods: Fundamentals and Applications, wiley, New York, 1980.
[37] H. Prifti, A. Parasuraman, S. Winardi, T.M. Lim, M. Skyllas-Kazacos, Membranes 2 (2012) 275–306, https://doi.org/10.3390/membranes2020275.
[38] X.-G. Yang, Q. Ye, P. Cheng, T.S. Zhao, Appl. Energy 145 (2015) 306–319, https://doi.org/10.1016/j.apenergy.2015.02.038.
[39] L. Hao, Y. Wang, Y. He, J. Electrochem. Soc. 166 (2019) A1310–A1322, https://doi.org/10.1149/2.1061906jes.
[40] X.-Z. Yuan, C. Song, A. Platt, N. Zhao, H. Wang, H. Li, K. Fatih, D. Jang, Int. J. Energy Res. 43 (2019) 6599–6638, https://doi.org/10.1002/er.4607.
[41] A. Thirunavukkarasu, R. Karunathan, J. Mallika, V. Sathyanarayanamoorthi, Indian J. Pure Appl. Phys. 52 (2015) 653–670. http://hdl.handle.net/123456789/29427.